Contents lists available at ScienceDirect

Nuclear Inst. and Methods in Physics Research, A

journal homepage: www.elsevier.com/locate/nima

Full Length Article

Anode capacitance measurement of silicon drift detectors in operating conditions

Giuseppe Bertuccio [a,b], Filippo Mele [a,b,*], Jacopo Quercia [a], Yongbiao Shi [a,c]

[a] *Politecnico di Milano - Department of Electronics, Information and Bioengineering, Como, Italy*
[b] *Italian National Institute of Nuclear Physics - INFN sez. Milano, Milan, Italy*
[c] *North China University of Water Resources and Electric Power, Zhengzhou, China*

ARTICLE INFO

ABSTRACT

We describe a technique for measuring with high accuracy and precision the capacitance of the anode of a semiconductor drift detector (SDD) fully biased in operating conditions and connected to the front-end electronics. The proposed method does not require the use of a probe station, making it suitable for low-cost and easy-to-setup application environments. We have performed measurements on four SDDs with different geometries and production processes, observing a total capacitance ranging from 20 fF to 75 fF, depending on the bias conditions. Different components of the anode capacitance with respect to the front cathode and the adjacent drift cathodes have been measured and commented as well. Precision in the capacitance measurements better than 0.1 fF has been obtained. These results can be effectively used for the optimization of the front-end electronics for SDDs to achieve minimum electronic noise.

1. Introduction

Silicon (or semiconductor) drift detectors (SDDs), proposed by E. Gatti and P. Rehak in 1983 [1], are today undoubtedly among the most used solid-state X-ray detectors for high energy-resolution spectroscopy applications. Monolithic SDDs of different topologies, sizes and geometries have been manufactured and successfully characterized: linear and cylindrical geometries with area ranging from few mm^2 up to tens of cm^2, single or multiple anodes, pixel arrays [2–6]. Several commercial spectrometers based on SDD are available as well [7–9]. Owing to the small-size (usually <0.01 mm^2) of the output electrode (anode) where the electrons are collected[1] and due to the fully depleted volume, the anode is characterized by a small capacitance (tens of fF) that is independent from the detector active area. This feature makes SDDs the preferred choice for detectors in the soft X-ray energy band (0.1–30 keV) for both experiments at synchrotrons [6,10,11], free-electron lasers (FEL) [3] and space-borne astrophysics applications [12–15] as well as for numerous industrial applications. Despite the low output capacitance of SDDs is widely reported in the scientific literature, most of these claims are based on geometrical evaluations and TCAD (Technology Computer Aided Design) simulations. The lack of experimental values of the anode capacitance can be attributed to the complex polarization scheme of SDDs, which requires at least 4

probe terminals in order to correctly bias all electrodes in the end-user operating conditions. A method based on multi-parameter fit of the equivalent noise charge data acquired at different shaping times allows to evaluate the total capacitance at the preamplifier input, but it requires the knowledge of some parameters related to electronics and all the other capacitive components (preamplifier, stray), in order to extract the detector's one [16]. In this paper we describe a method to effectively measure the SDD output capacitance in its functional operating conditions, when connected to the readout electronics. The proposed method does not require the use of a probe station, making it suitable for low-cost and easy-to-setup application environments. We show the measurements done on cylindrical SDDs, but the described method can be equivalently applied to any topology of SDD. Within our work we show the decomposition of the SDD total output capacitance as the sum of contributions from the first (inner) cathode, second cathode and front-cathode (also referred as entrance window electrode). The dependency with respect to the applied bias voltage is extracted and commented as well.

2. Methodology

In this section, the methodology to measure the output (anode) capacitance in operating conditions is presented. The methodology can
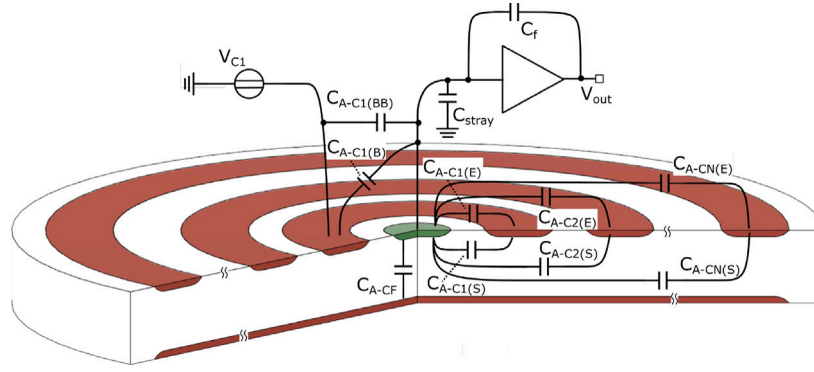

Fig. 1. Cross section of a cylindrical semiconductor drift detector. The capacitive coupling between the anode (in green) and the cathodes (in red) are indicated, distinguishing those through the semiconductor (S) from those through the external space (E), and those associated with the wire-bondings (B and BB). The stray capacitance between the anode bonding and ground (C_{stray}) is also represented.

be applied to any SDD geometry (linear, cylindrical, hexagonal etc.) as well as for single or double-sided SDDs [17]. Without any loss of generality, in our work we will consider a cylindrical structure, as schematized in Fig. 1; the detector's anode-side is constituted by a central n^+ implant (collecting anode), a series of p^+ ring cathodes, which realize the lateral drift field in the high-resistivity n-doped substrate. Eventually, an outer n^+ bulk contact is used to collect charges generated outside of the SDD active area (not shown in Fig. 1). The front-side of the SDD consists of a large, single electrode (front-cathode), which contributes to the semiconductor volume depletion. In operative conditions the bias of p^+ cathodes is set to fully deplete the detector's bulk of mobile charges, and to shape the electric potential in the characteristic gutter-like surface [18]. Typically, the front-cathode operates as the main entrance window for the incoming radiation.

As indicated in Fig. 1, the capacitance of the anode C_A is generated by the electrical coupling toward each cathode 1, 2,... N and toward the front cathode C_{A-CF}, that can be assumed to be all at signal ground. The capacitance of the anode C_{A-Cj} toward each j−cathode on the anode-side of the detector is the sum of:

- the capacitance between the anode and j−cathode electrodes $C_{A-Cj(S)}$, due to the coupling through the semiconductor.
- the capacitance between the anode and j−cathode electrodes $C_{A-Cj(E)}$, due to the coupling through the space (air or vacuum) external the detector.
- the capacitance between the anode bonding and the j−cathode electrode $C_{A-Cj(B)}$.
- the capacitance between the anode bonding and, if present, the j−cathode bonding $C_{A-Cj(BB)}$.

Summarizing, the anode capacitance is given by:

$$C_A = \sum_{j=1}^{c} (C_{A-Cj(S)} + C_{A-Cj(E)} + C_{A-Cj(B)} + C_{A-Cj(BB)}) + C_{A-CF} \qquad (1)$$

The measurement of C_A implies the experimental determination of all the capacitances in Eq. (1). It is worthwhile to consider that the wire bonding used to connect the anode to the preamplifier input, as any conductor connected to the preamplifier input itself (e.g. feedback network), constitutes a unique conductor together with the physical anode of the detector. Consequently, all the capacitances between the preamplifier input – including the wire bonding to the anode – and other AC-grounded electrodes belonging or not to the detector must be considered as components of the total stray capacitance C_{stray} in parallel to C_A.

To measure the anode-capacitance due to the x−electrode C_{A-Cx}, the detector is biased in operating condition, in order to fully deplete the detector volume and create the drift field towards the anode. The anode is connected to the charge sensitive amplifier (CSA), and the
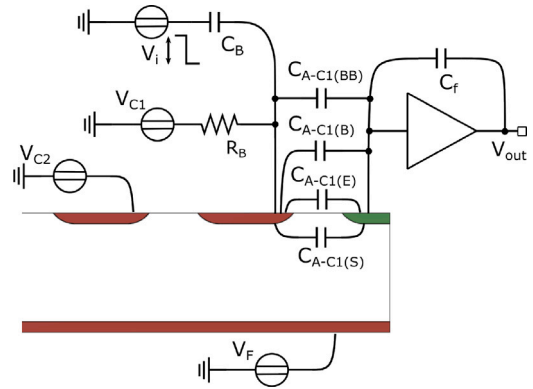

Fig. 2. Schematic circuit for the measurement of the total C_{A-C1} capacitance, using a precision pulser V_i and an AC-coupling network $R_B C_B$. All the capacitance contributions ($C_{A-C1(S)}$, $C_{A-C1(E)}$, $C_{A-C1(B)}$, $C_{A-C1(BB)}$) are measured at the same time. Similarly, the capacitance between the anode and any other electrode can be measured, applying the precision pulser through the AC-coupling network at the electrode of interest.

CSA output is sent to a shaper and a multi-channel analyzer (MCA), as typically done for a spectroscopic acquisition system. A precision pulser (V_i) is AC-coupled to the x−electrode under consideration, using a C_B capacitance in series with the pulser, and a R_B resistance in series with the V_{Cx} bias generator of the x−electrode itself. As an example, Fig. 2 schematically shows the principle of the measurement for the C_{A-C1} capacitance, associated with the first cathode ($x = 1$).

The precision pulser is used to generate a series of fast voltage steps of known amplitude ΔV_{inj} across the capacitance C_{A-Cx}.[2] A charge signal $Q_{inj} = C_{A-Cx} \cdot \Delta V_{inj}$ is thus injected at the CSA input, producing a pulser line in the MCA spectrum. At the same time, the SDD is irradiated with a known radioactive source (e.g. ^{55}Fe or ^{241}Am) from the entrance-window, and the spectrum of the radioactive source is acquired as well. Knowing the mean electron–hole pair generation energy of the semiconductor ε, and assuming a linear operation of the system, the radioactive calibration source and the injected charge signals will generate a series of spectral lines at channel number ch_i of the MCA, according to the relationship:

$$ch_i = a \cdot Q_i + b \qquad (2)$$

where Q_i is the charge injected at the CSA input, and a and b are constant values (gain and offset) characteristic of the readout system.

---

[2] These fast voltage steps, passing unaltered through C_B, should be sufficiently small, so as not to modify the bias operating condition of the x−electrode.
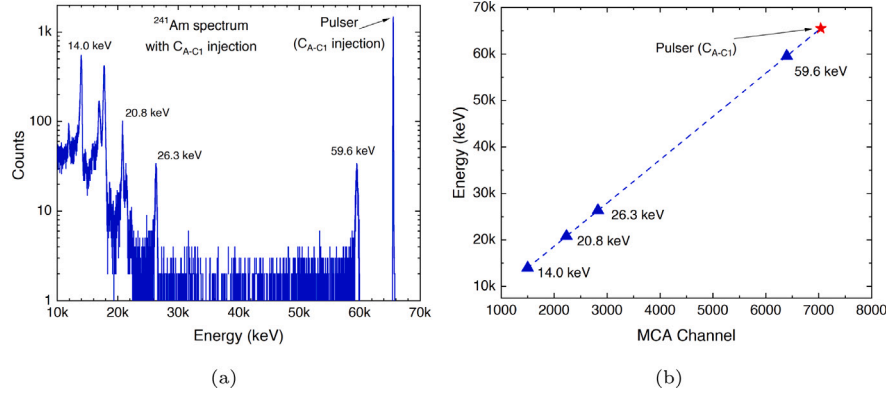
(a)   (b)

Fig. 3. In (a), an example of an acquired calibrated spectrum for the C_{A-C1} capacitance measurement using a 370 kBq ^{241}Am source, placed at 1 cm from the detector. The pulser operates at 500 pulse per seconds generating the line at ∼65 keV. In (b) the linear fit of the centroids of the ^{241}Am lines and of the pulser is used to compute the capacitance under measurement.
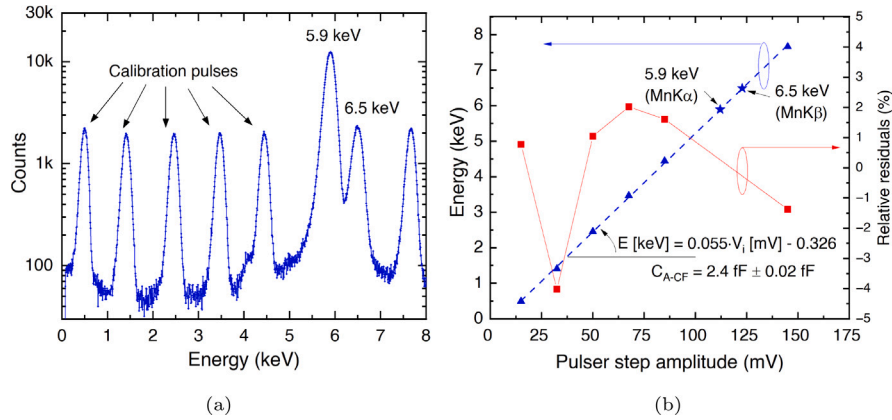

(a)   (b)

Fig. 4. In (a), an example of an acquired calibration spectrum with the ^{55}Fe source, and the several calibration pulses (5 at lower energies and 1 at a higher energy). In (b) the centroids of the pulser and Mn-K lines are used to derive with high accuracy the C_{A-CF} capacitance.

As known, the acquisition of a spectrum from a radioactive source having at least two monoenergetic lines allows to determine a and b. Thus, the so-called "calibrated" energy spectrum can be reconstructed, as shown in Fig. 3(a) for the C_{A-C1} measurement using a ^{241}Am source. Measuring the calibrated energy centroids E_{inj} of the pulser line, we can draw the calibration plot (Fig. 3(b)), according to the following equation:

$$E_{inj} = \varepsilon \cdot Q_{inj} = \varepsilon \cdot C_{A-Cx} \cdot \Delta V_{inj} \tag{3}$$

Finally, the desired value of the capacitance C_{A-Cx} can extracted by least square linear fit. For extremely small capacitance values, the injection of multiple peaks allows a more accurate measurement, as shown in Fig. 4 for the front-cathode measurement C_{A-CF}, where the presence of an eventual offset term can be corrected as well. In this case, a sufficiently uniform distribution of residuals over the fitted points allows to assess the validity of the linearity assumption, as shown on the right-Y axis of Fig. 4(b). It can be observed as capacitance values as low as a few femtofarads can be measured with a precision of tens of attofarads.

3. Anode capacitance measurement in operating conditions

In this section, the anode capacitance measurement results obtained for four different SDDs are presented. The SDD samples are taken from two different manufacturer (Fab-1 and Fab-2 in the following). All SDDs are cylindrical but characterized by different geometries and manufacturing processes. In all the measurements, for the charge readout, the SIRIO CSA has been used [19,20], connecting the anode
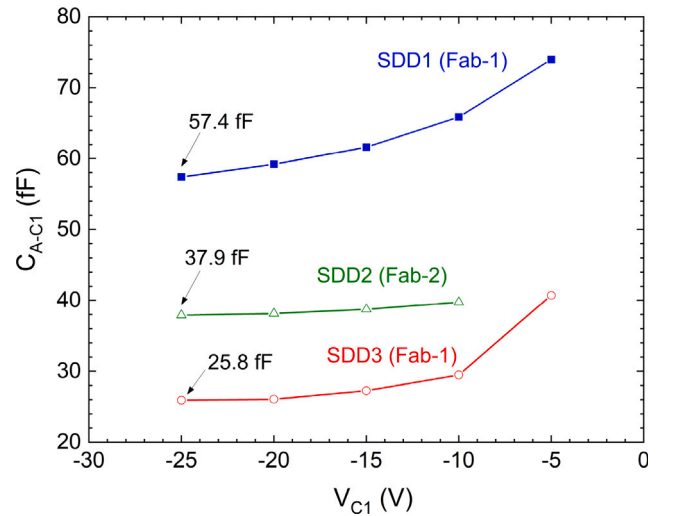

Fig. 5. Measurement of the component C_{A-C1} of the anode capacitance as function of the bias voltage at the first cathode V_{C1} for three different SDDs with an integrated resistive divider.

with a 25 μm aluminum wire bonding. The R_B and C_B values are chosen to obtain a time constant sufficiently longer than the peaking time of the shaper. In our setup, a shaping time of 1 μs was used, and $R_B C_B$ is several hundreds of microseconds. For three SDDs, in Fig. 5
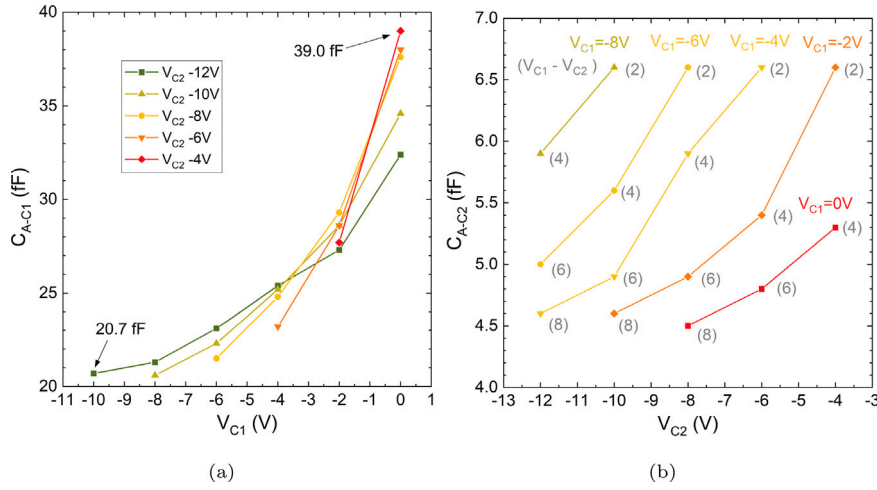
Fig. 6. Experimental data acquired on SDD4 with an additional bonding pad to independently bias the second cathode. In (a) the measurement results of the component C_{A-C1} of the anode capacitance with respect to the first cathode as a function of the bias of the first cathode itself, and with the bias voltage of the second cathode as parameter. In (b) the C_{A-C2} values are represented as function of the bias voltage at the second cathode V_{C2} with the first cathode bias V_{C1} as parameter.

the anode contribution measured by pulsing from the first (innermost) cathode are presented, with respect to the DC voltage bias applied on the first cathode itself. It should be also noted that, if the bias voltage of the drift cathodes is provided using an integrated resistive divider, as done in our case and in most SDD productions [21], the voltage step applied to the first cathode can propagate to all the other cathodes C_j through a distributed RC line. The cathodes nearest to the anode can so contribute, according to the voltage partition determined by the integrated resistive divider, to the total charge injected into the anode itself through their capacitances C_{A-Cj}. If the signal processing time is chosen larger than the expected risetime of the voltage step at the closest C_j due to the RC line, the measured C_A value will include the contributions from C_{A-Cj}, as well.

Experimental results reported in Fig. 5 show that the anode capacitance toward the nearest cathode ranges from 57.4 fF to 74 fF on SDD1, from 37.9 fF to 39.8 fF for the SDD2 and from 25.9 to 40.7 fF for SDD3, depending on the bias condition. As shown, a higher (i.e. more negative) bias voltage results in a lower anode capacitance toward the first cathode, in accordance with the expected increase of the depletion width around the anode superficial region. A measurement of the C_{A-CF} capacitance between the anode and the front-electrode of SDD3 shows an additional contribution of 2.4 fF as shown in Fig. 4(b). The measured value is close to the expected one determined by an anode contact area of 7×10^3 μm^2 at a distance of 300 µm from the front electrode. Since different SDDs have similar anode areas and tipical thicknesses between 300 µm and 500 µm, a C_{A-CF} capacitance lower than a few fF is expected for all the SDDs, not strongly affecting the final C_A value.

Taking into consideration an additional sample SDD4 we also had the possibility to separately set the bias voltage at the second cathode. This allows to separately measure C_{A-C1} and C_{A-C2}, observing the effect of the bias voltages applied to the two cathodes nearest to the anode. In addition, since the resistive divider is not present between the cathodes $C1$ and $C2$, the C_{A-C1} measurement is not affected by the contributions of all the other cathodes.

Fig. 6(a) shows the results of the measurement of the capacitance C_{A-C1} between the anode and the cathode 1 as a function of the voltage applied to cathode 1 and with cathode 2 bias as parameter. It can be observed that the anode capacitance toward the nearest cathode ranges 39.0 fF to 20.7 fF. Moreover, the variation of C_{A-C1} with respect to V_{C1} is quite significant because a factor of two of reduction of C_{A-C1} has been measured for V_{C1} changing from 0 V to −10 V. Again, this variation can be related to the reduction of the volume and the surface of the undepleted region surrounding the $n+$ anode itself, so

reducing the effective anode area. This dependency clearly indicates a sub-optimal bias for values of V_{C1} higher than 6 V in absolute value. In addition, a dependence of C_{A-C1} with respect to the voltage applied to the second cathode V_{C2} is also observed. This effect can be explained by assuming that the surface and the volume around the anode is only partially depleted and that the C_2 bias can affect their depletion. This justifies why the maximum effect is seen for $V_{C1} = 0$ V giving a variation of 16% of C_{A-C1} for V_{C2} ranging from −4 V to −12 V. At higher V_{C1}, the variations are much smaller in absolute value, less than 10%, but also of opposite sign: C_{A-C1} increases with the decreasing of V_{C2}. While the decreasing of C_{A-C1} with V_{C2} can be expected due to a deeper depletion close to the anode, the opposite behavior is not clear. Anyhow, it has been observed that the measured variations of C_{A-C1} are less than 2 fF for $V_{C2} \leq -6V$.

Similarly, Fig. 6(b) shows the results of the measurement of the capacitance C_{A-C2} between the anode and the cathode 2 as a function of the voltage applied to cathode 2 and with cathode 1 bias as parameter. This capacitance ranges between 4.5 fF and 6.5 fF for all the measuring range, as can be observed. Although the absolute value of this capacitance is rather small with respect to C_{A-C1}, its dependence on both V_{C1} and V_{C2} is relatively significant. it can be observed that C_{A-C2} remains practically constant for equal potential differences $V_{C1} - V_{C2}$ between the cathode and decreases as $V_{C1} - V_{C2}$ increases. Since the increasing of $V_{C1} - V_{C2}$ determines a wider depletion of the surface between the two cathodes, it can be argued that the residual conductive surface layer between the cathode contributes to the capacitive coupling between the cathode 2 and the anode.

It can be observed that the C_{A-C1} between the anode and the first cathode ring is the dominant component of the anode capacitance, as expected, although the contribution of the second cathode cannot be completely neglected in some cases.

4. Conclusions

The output capacitance of a radiation detector is one of the most important parameters in the design of the radiation detection systems [22]. The front-end electronics optimization strongly relies on an accurate estimation of the detector, interconnection and stray capacitances at the preamplifier input. In this work we presented a high-precision measurement methodology for the anode capacitance of Semiconductor Drift Detectors in operative conditions, connected to a standard signal acquisition system constituted by a charge sensitive amplifier, a shaper and a multi-channel analyzer. Experimental results

have been reported on four different SDDs, characterized by different geometries and manufacturing processes, showing a total output capacitance between 20 fF and 75 fF, emphasizing in some cases a significant dependency on the bias conditions. The method demonstrated to be able to measure capacitance of a few fF, as the anode-window capacitance, with precision of few tens of attofarads.

CRediT authorship contribution statement

Giuseppe Bertuccio: Writing – review & editing, Writing – original draft, Supervision, Resources, Project administration, Methodology, Investigation, Funding acquisition, Formal analysis, Conceptualization. **Filippo Mele:** Writing – review & editing, Writing – original draft, Visualization, Supervision, Software, Methodology, Formal analysis, Data curation, Conceptualization. **Jacopo Quercia:** Visualization, Software, Investigation, Data curation. **Yongbiao Shi:** Investigation, Formal analysis, Data curation.

Declaration of competing interest

The authors declare that they have no known competing financial interests or personal relationships that could have appeared to influence the work reported in this paper.

Data availability

Data will be made available on request.

Acknowledgments

References

[1] E. Gatti, P. Rehak, Semiconductor drift chamber—An application of a novel charge transport scheme, Nucl. Instrum. Methods Phys. Res. 225 (3) (1984) 608–614, http://dx.doi.org/10.1016/0167-5087(84)90113-3.

[2] G. Utica, E. Fabbrica, M. Carminati, G. Borghi, N. Zorzi, F. Ficorella, A. Picciotto, I. Allegretta, G. Falkenberg, C. Fiorini, ARDESIA-16: a 16-channel SDD-based spectrometer for energy dispersive X-ray fluorescence spectroscopy, J. Instrum. 16 (07) (2021) P07057.

[3] M. Porro, L. Andricek, S. Aschauer, A. Castoldi, M. Donato, J. Engelke, F. Erdinger, C. Fiorini, P. Fischer, H. Graafsma, et al., The MiniSDD-based 1-mpixel camera of the DSSC project for the European XFEL, IEEE Trans. Nucl. Sci. 68 (6) (2021) 1334–1350.

[4] F. Ceraudo, F. Ambrosino, P. Bellutti, G. Bertuccio, G. Borghi, R. Campana, M. Caselle, D. Cirrincione, I. Dedolli, E. Del Monte, et al., Pixdd: a multi-pixel silicon drift detector for high-throughput spectral-timing studies, in: X-Ray, Optical, and Infrared Detectors for Astronomy X, Vol. 12191, SPIE, 2022, pp. 396–406.

[5] M. Feroci, G. Ambrosi, F. Ambrosino, M. Antonelli, A. Argan, V. Babinec, M. Barbera, J. Bayer, P. Bellutti, B. Bertucci, et al., The large area detector onboard the extp mission, in: Space Telescopes and Instrumentation 2022: Ultraviolet To Gamma Ray, Vol. 12181, SPIE, 2022, pp. 466–483.

[6] D. Cirrincione, M. Antonelli, G. Aquilanti, P. Bellutti, G. Bertuccio, G. Borghi, G. Cautero, F. Ficorella, M. Gandola, D. Giuressi, et al., A new collimated multichannel modular detection system based on silicon drift detectors, Nucl. Instrum. Methods Phys. Res. A 1049 (2023) 168118.

[7] S. Barkan, J.S. Iwanczyk, B.E. Patt, L. Feng, C.R. Tull, G. Vilkelis, Vortex-a new high performance silicon drift detector for xrd and xrf applications, Adv. X-Ray Anal. 46 (2003) 332–337.

[8] A. Pahlke, F. Dams, R. Fojt, M. Fraczek, L. Höllt, J. Knobloch, N. Miyakawa, High performance silicon drift detectors for energy dispersive spectroscopy, Microsc. Microanal. 24 (S1) (2018) 1150–1151.

[9] R. Redus, A. Huber, J. Pantazis, T. Pantazis, Enhanced energy range thermoelectrically cooled silicon X-ray detectors, in: 2011 IEEE Nuclear Science Symposium Conference Record, IEEE, 2011, pp. 580–585.

[10] A. Vacchi, D. Cirrincione, M. Altissimo, M. Antonelli, G. Aquilanti, P. Bellutti, G. Bertuccio, G. Borghi, I. Carlomagno, G. Cautero, et al., Recent progress in high resolution X-ray customised detection systems, in: Journal of Physics: Conference Series, Vol. 2380, IOP Publishing, 2022, 012095, (1).

[11] A. Rachevski, M. Ahangarianabhari, G. Aquilanti, P. Bellutti, G. Bertuccio, G. Borghi, J. Bufon, G. Cautero, S. Ciano, A. Cicuttin, et al., The XAFS fluorescence detector system based on 64 silicon drift detectors for the SESAME synchrotron light source, Nucl. Instrum. Methods Phys. Res. A 936 (2019) 719–721.

[12] F. Mele, I. Dedolli, M. Gandola, M. Grassi, P. Malcovati, L. Amati, P. Bellutti, G. Borghi, R. Campana, E. Demenev, et al., ORION, a multichip readout electronics for satellite wide energy range X-/γ-ray imaging spectroscopy: Design and characterization of the analog section, IEEE Trans. Nucl. Sci. 68 (12) (2021) 2801–2809.

[13] M. Gandola, M. Grassi, F. Mele, P. Malcovati, G. Bertuccio, LYRA: a multi-chip ASIC designed for HERMES X and gamma ray detector, in: 2019 IEEE Nuclear Science Symposium and Medical Imaging Conference (NSS/MIC), IEEE, 2019, pp. 1–3.

[14] M. Gandola, M. Grassi, F. Mele, I. Dedolli, P. Malcovati, G. Bertuccio, The sparse readout RIGEL application specific integrated circuit for pixel silicon drift detectors in soft X-ray imaging space applications, Nucl. Instrum. Methods Phys. Res. A 1040 (2022) 167249.

[15] Y. Evangelista, F. Ambrosino, M. Feroci, P. Bellutti, G. Bertuccio, G. Borghi, R. Campana, M. Caselle, D. Cirrincione, F. Ficorella, et al., Characterization of a novel pixelated silicon drift detector (PixDD) for high-throughput x-ray astrophysics, J. Instrum. 13 (09) (2018) P09011.

[16] G. Bertuccio, A. Pullia, A method for the determination of the noise parameters in preamplifying systems for semiconductor radiation detectors, Rev. Sci. Instrum. 64 (11) (1993) 3294–3298.

[17] L. Wang, W. Luo, R. Jia, K. Tao, D. Zhang, B. Wang, X. Li, Design and fabrication of quasi-double-sided silicon drift detector for x-ray detection, Mater. Sci. Semicond. Process. 155 (2023) 107201.

[18] P. Rehak, E. Gatti, A. Longoni, J. Kemmer, P. Holl, R. Klanner, G. Lutz, A. Wylie, Semiconductor drift chambers for position and energy measurements, Nucl. Instrum. Methods Phys. Res. A 235 (2) (1985) 224–234.

[19] F. Mele, M. Gandola, G. Bertuccio, SIRIO: A high-speed CMOS charge-sensitive amplifier for high-energy-resolution X-γ ray spectroscopy with semiconductor detectors, IEEE Trans. Nucl. Sci. 68 (3) (2021) 379–383.

[20] M. Sammartini, M. Gandola, F. Mele, G. Bertuccio, F. Ambrosino, P. Bellutti, G. Borghi, R. Campana, M. Caselle, D. Cirrincione, et al., Pixel drift detector (pixdd)–SIRIO: An X-ray spectroscopic system with high energy resolution at room temperature, Nucl. Instrum. Methods Phys. Res. A 953 (2020) 163114.

[21] C. Fiorini, A. Longoni, P. Lechner, Single-side biasing of silicon drift detectors with homogeneous light-entrance window, IEEE Trans. Nucl. Sci. 47 (4) (2000) 1691–1695.

[22] G. Bertuccio, F. Mele, Electronic noise in semiconductor-based radiation detection systems: a comprehensive analysis with a unified approach, IEEE Trans. Nucl. Sci. 70 (10) (2023) 2310–2321.